Effect of the Burner Arrangement on Slab Reheating Characteristics in a Reheating Furnace

Yiwei Liu[a], Jin Wang[a],*, Wei Wang[b], Ran Yang[c], Chunhua Min[a], Bengt Sundén[d]

[a]School of Energy and Environmental Engineering, Hebei University of Technology, Tianjin 300401, China
[b]Experimental Training Center, Hebei University of Technology, Tianjin 300401, China
[c]PERA GLOBAL, Ltd., Beijing 100025, China
[d]Department of Energy Sciences, Division of Heat Transfer, Lund University, Lund SE-22100, Sweden
 wjwcn00@163.com

Slab reheating characteristics in the walking beam type reheating furnace were studied by using the finite volume method (FVM). A geometry model for simulating the gas circulation, heat transfer and slabs reheating process in a reheating furnace was developed by using ANSYS FLUENT software. Usually, slabs are heated in the furnace, and temperature values of the slabs reach above 1,500 K. After that, they are transported to the rolling mill. The slab reheating in a reheating furnace is influenced by many factors, such as gas velocity, moving speed of the slabs, and burner arrangement. Especially, the arrangement of burners shows a great effect on reheating the slabs. In the paper, the main object of study is to investigate the temperature distribution in the reheating furnace by considering the effect of the burner position. In addition, it is found that the temperature fields of the slabs are significantly affected by changing the positions of the burners.

1. Introduction

Industrial furnace is one of important reheating equipment and widely used in various industrial fields. To improve quality of products and reduce the energy consumption, many studies focus on the temperature distribution inside the furnace. Numerical simulations are used to model and solve the slab reheating process. A 3 MW industrial furnace was with low NOx burners combustion test model investigated by using computational fluid dynamics (CFD), and Galletti et al. (2013) recommended to use an oxygen fuel spectrum model. Park et al. (2015) simulated temperature and velocity fields inside a furnace. The results showed that change of the jet Angle had a significant impact on the gas temperature and flow fields. Han et al. (2011) calculated radiation heat exchanges by using the finite volume method, and they also calculated slab temperature field with the transient heat conduction equation. Jang et al. (2010) introduced the development of reheating furnace mathematical model. The results showed that the slab heating effect is significant. Kim et al. (2010) calculated the radiant heat flux in a furnace by FVM, and the billet temperature distribution was obtained. Han et al. (2012) studied the billet reheating characteristics by a user defined function (UDF) program. They also handled the fast moving of slabs. It showed that the main reheating areas of the slabs appear in preheating and reheating zones. In addition, the temperature increase in the soaking zone is small.

In the paper, the temperature distribution inside the furnace and on the slabs isbe discussed in detail. The slab moving is handled by using UDF program in ANSYS FLUENT 17.2.

2. Geometry model

All the cases are calculated based on the same geometry model as shown in Fig.1. Because geometry and physical phenomena are symmetrical, half a reheating furnace was used to reduce the computational resources. The symmetry boundary is located at the plane z = 0. The dimensions of the computational domain are 34.8 m x 5.02 m x 5.4 m, and 29 slabs are included. The furnace contains three zones: preheating zone with 13 slabs, reheating zone with 9 slabs, and soaking zone with 7 slabs. Slabs enter the furnace and pass through the preheating, reheating and soaking zones in sequence. The furnace is equipped with 13 side burners in the lower

zone and 12 axial burners in the upper zone. Each burner was simplified by using concentric circles. The central zone and an annulus zone represent the fuel passage and the air passage. The diameters of the outer and inner circles are 0.5 m (D_1) and 0.25 m (D_2).
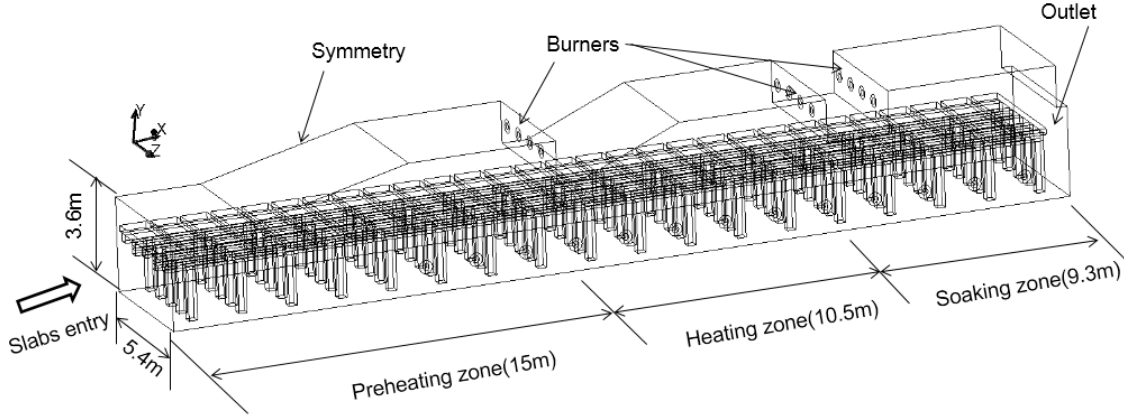
Figure 1: Geometry and computational domain.

3. Governing equations

The flow field in the furnace is transient and simulated by the three-dimensional Favre-averaged Navier-Stokes equations. The k-ε turbulence model was used for all the cases. All the variables in the original conservation equations are divided into the Favre-averaged and fluctuating components as:

$$\phi = \tilde{\phi} + \phi''$$

(1)

Then the Favre-averaged continuity and momentum equations can be written as:

$$\frac{\partial \overline{\rho}}{\partial t} + \frac{\partial \overline{\rho} \tilde{u}_i}{\partial x_i} = 0$$

(2)

$$\frac{\partial \overline{\rho} \tilde{u}_i}{\partial t} + \frac{\partial \overline{\rho} \tilde{u}_i \tilde{u}_j}{\partial x_j} = \frac{\partial}{\partial x_j}\left[\mu\left(\frac{\partial \tilde{u}_i}{\partial x_j} + \frac{\partial \tilde{u}_j}{\partial x_i} \right) - \left(\frac{2}{3}\mu \frac{\partial \tilde{u}_l}{\partial x_l} \right) \right] - \frac{\partial \overline{p}}{\partial x_i} + \frac{\partial}{\partial x_j}\left(-\overline{\rho u_i'' u_j''} \right)$$

(3)

The turbulent kinetic energy (k) and dissipation rate (ε) are given as:

$$\frac{\partial \overline{\rho} \tilde{k}}{\partial t} + \frac{\partial \overline{\rho} \tilde{u}_i \tilde{k}}{\partial x_i} = \frac{\partial}{\partial x_i}\left[\left(\mu + \frac{\mu_t}{\sigma_k} \right) \frac{\partial \tilde{k}}{\partial x_i} \right] - \overline{\rho u_i'' u_j''}\frac{\partial \tilde{u}_j}{\partial x_i} + \beta g_i \frac{\mu_t}{\text{Pr}_t}\frac{\partial \tilde{T}}{\partial x_i} - \overline{\rho}\tilde{\varepsilon}$$

(4)

$$\frac{\partial \overline{\rho} \tilde{\varepsilon}}{\partial t} + \frac{\partial \overline{\rho} \tilde{u}_i \tilde{\varepsilon}}{\partial x_i} = \frac{\partial}{\partial x_i}\left[\left(\mu + \frac{\mu_t}{\sigma_\varepsilon} \right) \frac{\partial \tilde{\varepsilon}}{\partial x_i} \right] - C_{2\varepsilon}\overline{\rho}\frac{\tilde{\varepsilon}^2}{\tilde{k}} + C_{1\varepsilon}\frac{\tilde{\varepsilon}}{\tilde{k}}\left[-\overline{\rho u_i'' u_j''}\frac{\partial \tilde{u}_j}{\partial x_i} + \left(1 - C_{3\varepsilon} \right)\beta g_i \frac{\mu_t}{\text{Pr}_t}\frac{\partial \tilde{T}}{\partial x_i} \right]$$

(5)

Detailed information can be found in Wang et al. (2017).

4. Boundary conditions

The symmetry and outlets boundaries are specified to Neuman boundary condition. Flow variables are given at all of the burner inlets for both air and fuel streams, including mass flow rate, turbulent intensity, and turbulent viscosity ratio. There are three cases with different positions of the burners. The basic case (Case-A) has burners at one level. For the Case-B, the even burner in the preheating section is lifted by $0.5D_2$, and the even burners in the reheating section are lifted by $0.5D_2$, $0.6D_2$, and $0.7D_2$, successively. The even burners are lifted by $0.5D_2$, $0.6D_2$ in the soaking section, successively. For the Case-C, the burner positions are lifted by $0.5D_2$, $0.6D_2$, $0.7D_2$ both from the inlet and outlet of the furnaces, successively. The air swirls at the inlets are ignored, i.e., all of the air and the fuel are supposed to enter into the furnace vertically. All the walls are stationary with no slip wall boundary condition. Information of fuel composition is shown in Table 1.

Table 1: Fuel composition.

Species	Mass fraction
CH_4	0.132
C_2H_6	0.022
H_2	0.039
CO_2	0.258
CO	0.183
O_2	0.007
N_2	0.359

5. Thermal properties

The dynamic process of the slabs feeding into the furnace is assumed that all the slabs are statically arranged in the furnace with ignoring the time for moving slabs. Temperature values were periodically transferred from the previous location to the next one by scheme commands in FLUENT. In order to consider the effect of the position on the thermo-physical properties of slab, thermal properties during simulations are assigned to 29 slabs according to values as shown in Table 2. The density of slab is constant, i.e., 7854 kg/m^3. The absorption coefficient for the mixed gas is processed by the weighted-sum-of-gray-gases model.

Table 2: Slab thermal properties.

Temperature (K)	Conductivity (W/m K)	Specific heat (J/kg K)
T < 473	60.57	504.0
473 < T <673	51.17	577.9
673 < T <873	41.74	712.3
873 < T <1073	34.04	892.1
1073 < T <1273	28.08	730.8
T > 1273	29.81	672.0

6. Mesh and simulation

Figures and tables should be originals or sharp prints; they must be well readable without enlarging with the zoom. Illustrations will be in colour in the electronic version and black and white in case of printed version. The authors must make sure that the figures are legible and understandable in greyscale mode. Avoid referencing your text to coloured items in the figures. All these means will be lost after the printing and will create Polyhedral meshes are used to discrete the computed domain, which brings higher computational efficiency and better convergence than tetrahedral meshes. Transient simulation depends on the results from steady state calculation. The steady state results are obtained when the residual levels are under 10^{-5}. The time step is 16 s, and a new slab is fed into the furnace every 256 s. Therefore, the total time with 29 slabs is 7,424 s. When the averaged slab temperature shows little difference, the calculation is considered to achieve the convergence within a time step. Han and Chang compare the result in this thesis, and it will verify three different the number of mesh model. For the average temperature of slabs, the average error is less than 200 K as shown in Fig. 2.
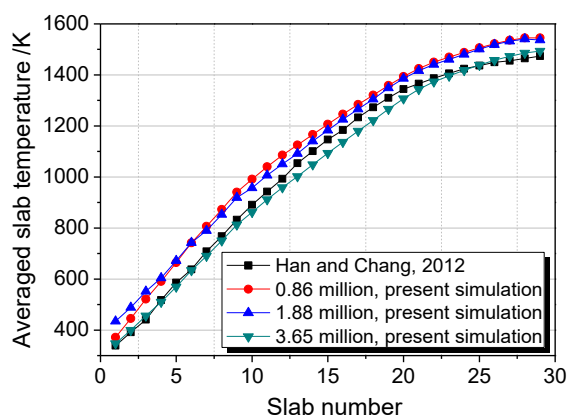
Figure 2: Grid independence and validation.

For the positions from the 7th slab to 19th slab, the case with 0.86 million cells shows larger deviations than results in Han and Chang (2012). To improve the quality of the grid, it has simulated the 1.88 M grid model. The first slab averaged temperature is not accurate, but the slabs in the middle of the furnace show good consistency. Although the results of 3.65 M cell case keep consistent with the other reference, there are some difference in the zone from 10th to 22nd slabs. Finally, the case with 1.88 M cells was used to save computational time and resources in this study.

7. Results and Discussion

With combustion in the furnace, the temperature field is periodic and unsteady. The whole reheating furnace is axial symmetry. The middle plane is located at $Z = 0$. Figure 3 shows the temperature distributions under different cases at $Z = 3.2D_2$. For the Case-B, low temperature range in the preheating section becomes smaller than the Case-A. For the Case-B, a higher temperature zone appears in the reheating section. For the Case-C, the temperature values in the soaking section are lower than that for the Case-B. Compared with the temperature values in the plane $Z = 3.2D_2$, both Case-B and Case-C show some improvements. Especially, the Case-B provides the best reheating efficiency.
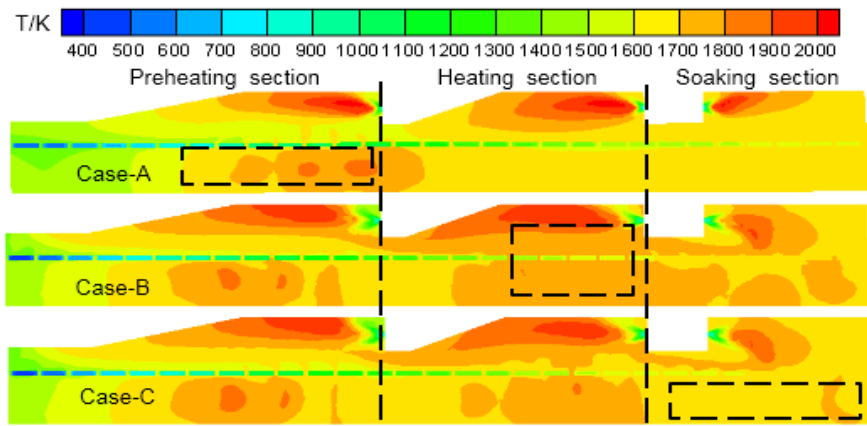
Figure 3: Temperature distributions for different cases at z = 3.2D_2.

Figure 4 shows the temperature distributions for different cases at the $y = 4D_2$. In Case-A, the temperature is uniform in the preheating section. The temperature of the furnace is high by the influence of the first burner in Case-B. The heating temperature in the heating section of Case-B is higher than that of Case-A, Case-C. The temperature field distribution is not uniform in the soaking section of Case-C, Case-B compared to Case-C, Case-B of temperature distribution is more even, temperature is higher, closer to the target temperature.
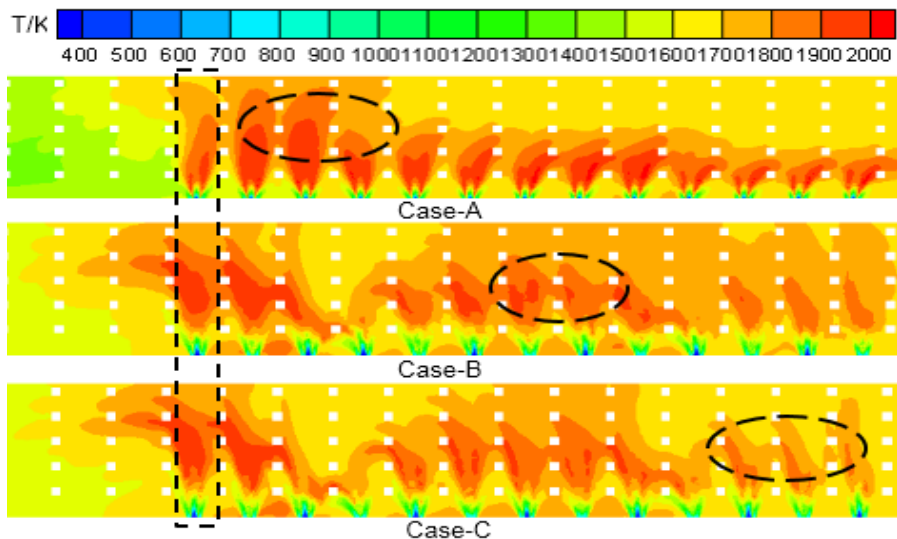
Figure 4: Temperature distributions for different cases at y = 4D_2.

In order to investigate the reheating efficiency of the burners in the upper region, the temperature distribution on the surface of the slab is analysed as shown in Fig. 5. The upper surface of the slab is continuously heated, and the new slab was inserted into the furnace from the inlet on the left. The average temperature value for the 2th slab reaches 600 K. The Case-C shows a lower temperature value near the 27th slab. Compared to the other cases, the Case-B provides a higher reheating efficiency especially after the 27th slab.
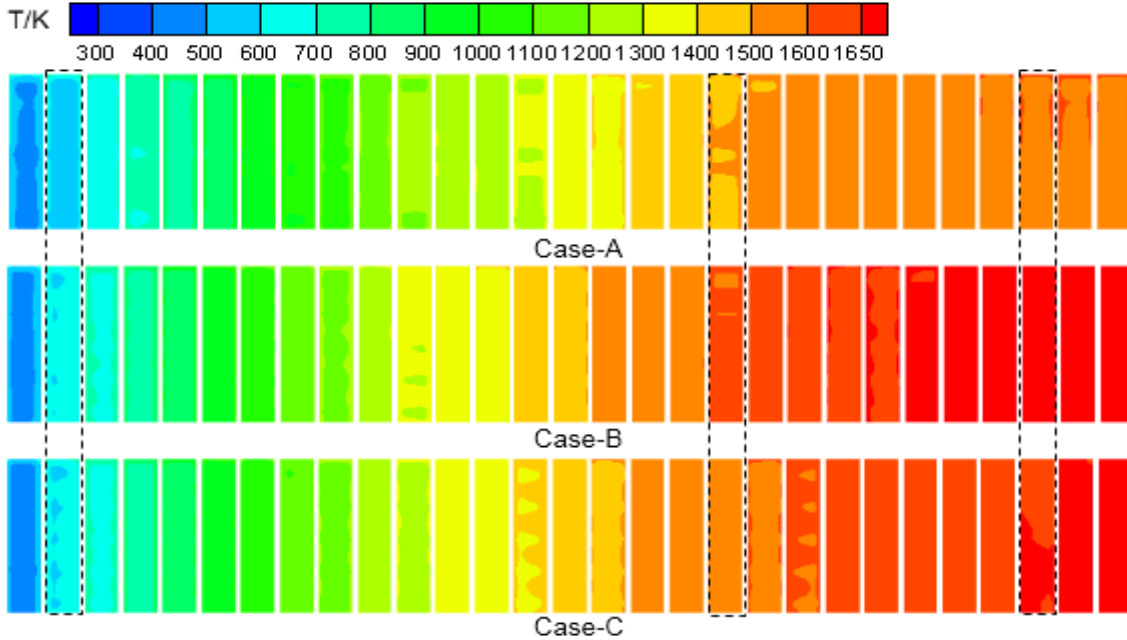
Figure 5: Temperature distributions on upper surfaces of slabs.

Figure 6 quantitatively shows the average temperature values of the upper slab surfaces. For the Case-A, the average temperature values have a slight decrease at the positions of the 22^{t}h and 23th slabs, which indicates that the reheating efficiency is reduced at the junction location of the reheating section and the soaking section. Considering the slab delivery in the preheating section for the Case-A, the slab surface temperature for the Case-B is about 1,320 K, while the average temperature for the Case-C is about 1,300 K. The average temperature for the 29th slab in Case-A and Case-C is about 1,600 K, while the average temperature for the Case-B is about 1,700 K. From the curves of the results, it indicates that the reheating efficiency of the upper burners for the Case-B is higher than those of the Case-A and the Case-C. In order to determine the comprehensive reheating efficiency, the volume averaged temperature is given in Fig. 6.
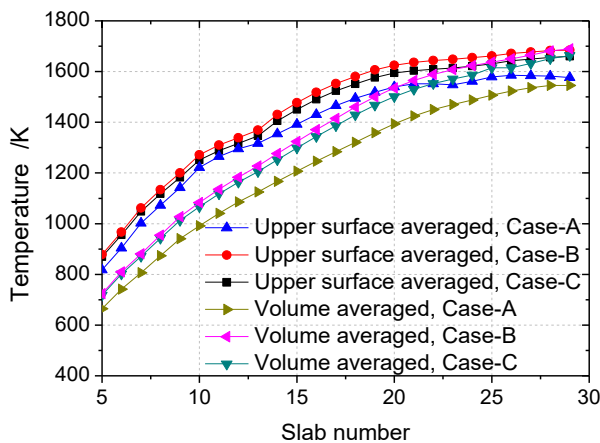
Figure 6: The upper surface and volume averaged temperature of each slab.

The Case-B shows higher reheating efficiencies in three regions than those for the Case-A and Case-C. The volume averaged temperature for the Case-B is about 1,700 K. Compared with the results from the Case-B and the Case-C, the volume averaged temperature for the Case-A is very low. The Case-B shows the highest volume averaged slab temperature and the best reheating efficiency.

8. Conclusions

In this research, the results from the unsteady-state calculation were based on the steady-state calculations. The slab reheating characteristics were investigated for different arrangements of burners. Program command streams were used to complete all the simulations. Main conclusions were obtained as follows: The average slab temperature on the upper surface are reduced at the transition region between the reheating section and the soaking section in the Case-A; the average slab temperature values in three regions show an increasing trend; compared with the other two cases, the Case-B provides the highest average temperature and reheating efficiency.

Acknowledgments

References

Galletti C., Coraggio G., Tognotti L., 2013, Numerical Investigation of Oxy-natural-gas Combustion in a Semi-industrial Furnace: Validation of CFD Sub-models, Fuel, 109(7), 445-460.

Han S.H., Chang D., 2012, Optimum Residence Time Analysis for a Walking Beam Type Reheating Furnace, International Journal of Heat and Mass Transfer, 55(15–16), 4079-4087.

Han S.H., Chang D., Huh C., 2011, Efficiency Analysis of Radiative Slab Reheating in a Working Beam Type Reheating Furnace, Energy, 36(2011), 1265-1272.

Jang J.H., Dong E.L., Man Y.K., Kim H.G., Investigation of the Slab Reheating Characteristics in a Reheating Furnace with the Formation and Growth of Scale on the Slab Surface, International Journal of Heat and Mass Transfer, 53(53), 4326-4332.

Kim J.G., Kang Y.H., Kim I.T., 2010, Three-Dimensional Analysis of the Walking Beam-Type Slab Reheating Furnace in Hot Strip Mills, Numerical Heat Transfer, Part A: Applications, 38(6), 589-609.

Park H.Y., Baek S.Y., Kim H.H., Kim Y.J., Kim T.H., Lim H.S., Kang D.S., 2015, Reduction of Main Steam Temperature Deviation in a Tangentially Coal-fired Two Pass Boiler, Fuel, 166(3), 509-516.

Wang J., Liu Y.W., Sundén B., Yang R., Baleta J., Vujanović M., 2017, Analysis of Slab Heating Characteristics in a Reheating Furnace, Energy Conversion and Management, DOI: 10.1016/j.enconman.2017.04.005.